Neurobiology of Disease 212 (2025) 106973

Contents lists available at ScienceDirect

Neurobiology of Disease

journal homepage: www.elsevier.com/locate/ynbdi

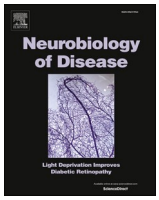

Exploring the impact of SerpinA3n deficiency on prion strains propagation

Fabio Moda [a,b,1], Chiara Ferracin [c,1], Ilaria Linda Dellarole [b], Edoardo Bistaffa [d], Chiara Maria Giulia De Luca [d], Marco Zattoni [c], Diletta Giovanna Legari [e], Lea Nikolic [c], Anna Burato [c], Martina Brce [c], Giuseppe Bufano [b,f], Merve Begüm Bacınoğlu [b], Federico Angelo Cazzaniga [b], Tihana Lenac Rovis [g], Giuseppe Legname [c,h,*]

[a] Department of Medical Biotechnology and Translational Medicine, University of Milan, Milan, Italy
[b] Unit of Laboratory Medicine – Laboratory of Clinical Pathology, Fondazione IRCCS Istituto Neurologico Carlo Besta, Milan, Italy
[c] Laboratory of Prion Biology, Department of Neuroscience, Scuola Internazionale Superiore di Studi Avanzati (SISSA), Trieste, Italy
[d] Unit of Neurology 5 and Neuropathology - Fondazione IRCCS Istituto Neurologico Carlo Besta, Milan, Italy
[e] Eurospital SPA, Trieste, Italy
[f] Department of Medicine and Surgery, University of Milano-Bicocca, Milan, Italy
[g] Center for Proteomics, Faculty of Medicine, University of Rijeka, Rijeka, Croatia
[h] ELETTRA Sincrotrone Trieste S.C.p.A, Basovizza, Trieste, Italy

ARTICLE INFO

Keywords:
Prion diseases
Serpin
SerpinA3n
SERPINA3
PMCA
Neurodegeneration

ABSTRACT

Transmissible spongiform encephalopathies (TSEs) are a group of devastating neurodegenerative diseases characterized by the conversion of the normal cellular prion protein (PrP^{C}) into its misfolded, pathogenic form, PrP^{Sc}. Despite significant research, the exact molecular mechanisms driving PrP^{C} to PrP^{Sc} conversion remain elusive and are thought to involve multiple molecules or cofactors. One protein of interest, SERPINA3 (murine SerpinA3n), is an acute-phase protein, a member of the serine protease inhibitor family. Intriguingly, SERPINA3 expression is notably upregulated in the brains of patients with Creutzfeldt-Jakob disease and in mice experimentally infected with prions, suggesting a potential role in prion disease pathology. In this study, we deepened the role of SerpinA3n in prion conversion and propagation by utilizing SerpinA3n-deficient ($SerpinA3n^{-/-}$) mice intracerebrally injected with the RML, 139A, or ME7 prion strains. Our results showed that the specific absence of SerpinA3n did not significantly affect prion propagation, as evidenced by the lack of notable changes in clinical and neuropathological assessments. Compensatory mechanisms involving other serpins or molecules may mitigate the effects of the specific absence of SerpinA3n, thereby maintaining efficient prion propagation.

1. Introduction

Prions (PrP^{Sc}) are pathogenic proteins responsible for a group of incurable neurodegenerative diseases (NDs) named transmissible spongiform encephalopathies (TSEs) (Sejvar et al., 2008). TSEs are caused by the conversion of the normal cellular prion protein (PrP^{C}), a glycoprotein typically expressed in the central nervous system (CNS), into its misfolded, disease-associated form, PrP^{Sc} (Aguzzi, 2006; Chesebro, 1999; Bodemer, 2016). PrP^{C} contains two N-linked glycosylation sites (at asparagine residues 181 and 197), which give rise to three different PrP species: diglycosylated, monoglycosylated, and unglycosylated (Turk et al., 1988). While PrP^{C} is sensitive to protease digestion and is soluble in mild detergents, PrP^{Sc} is rich in β-sheet structures, partially resistant to proteases degradation (C-terminal core of 27–30 kDa) and almost insoluble in detergents (Prusiner et al., 1998; Wulf et al., 2017). Prion strains can be distinguished by several key parameters, with the most prominent being incubation periods, patterns of neuropathological changes, and clinical symptoms. These *in vivo* characteristics serve as crucial markers for differentiating between various prion strains (Fraser, 1993). PrP^{Sc} derived from mouse-adapted scrapie prion strains, including RML, 139A and ME7 exhibits similar electrophoretic properties following proteinase K (PK) digestion. In all these strains, the unglycosylated PrP^{Sc} band has an electrophoretic mobility of approximately 21 kDa, and the glycosylation pattern (referred to as glycoform ratio) is comparable, with the monoglycosylated form being the most prominent (Kascsak et al., 1986; Rubenstein et al., 1991; Kascsak et al.,

* Corresponding author.
E-mail address: legname@sissa.it (G. Legname).
[1] These authors contributed equally to this work.

https://doi.org/10.1016/j.nbd.2025.106973
Received 24 March 2025; Received in revised form 9 May 2025; Accepted 22 May 2025
Available online 25 May 2025

1985; Morales et al., 2007). However, these strains can be distinguished by assessing the incubation time, the pattern of brain spongiform changes and the resistance to PK digestion after inoculation into mice (Morales et al., 2007; Fraser and Dickinson, 1973; Bruce et al., 1991; Solforosi et al., 2013). The exact molecular mechanisms which lead to PrP^{Sc} formation have not yet been clarified. Though, recent studies suggested the involvement of some molecules in prion pathology, including alpha-synuclein, peptidyl-prolyl isomerase 1 (Pin1) and some crucial protease inhibitors, known as serpins (Benetti et al., 2012; Legname et al., 2018; Bistaffa et al., 2019; Vanni et al., 2017; Zattoni et al., 2022). Serpins are widely distributed serine protease inhibitors, primarily produced in the liver but also synthesized in the brain by astrocytes. An imbalance in serpin levels can have serious consequences, contributing to various diseases (Baker, 2007). In particular, dysregulations of SERPINA3 (also known as α1-antichymotrypsin) have been linked to several diseases, including chronic obstructive pulmonary disease (COPD), cystic fibrosis, pancreatic cancer, prostate cancer, lung cancer, invasive breast cancer, and, more interestingly, to Alzheimer's (AD) and prion diseases (Zattoni et al., 2022; Baker, 2007; Elliott et al., 2000; Eriksson et al., 1986; Haass, 2004; D'Acunto et al., 2021; Mahadeva, 2001; Koomen et al., 2005; Leinonen et al., 1993; Higashiyama et al., 1995; Yamamura et al., 2004; Sun et al., 2002; Barbisin et al., 2014). SERPINA3 is a 56–66 kDa protein that can be glycosylated at several sites (Hwang et al., 1999) and is the only serpin capable of binding DNA, likely through repeat lysine motifs in the 210–212 and 391–396 regions (Naidoo et al., 1995). Its expression in astrocytes is strongly upregulated by IL-1, IL-6, and oncostatin M (Das and Potter, 1995; Kordula et al., 2000; Kordula et al., 1998). A microarray-based gene expression study performed by our group on the brain of macaques experimentally infected with bovine spongiform encephalopathy (BSE), revealed a significant up-regulation of SERPINA3 levels compared to healthy animals (Barbisin et al., 2014). Interestingly, elevated levels of SERPINA3 have been observed in the CNS, cerebrospinal fluid (CSF) and even urine of patients with sporadic Creutzfeldt-Jakob disease (sCJD) (Miele et al., 2008). In 2017, we examined SERPINA3 transcript and protein levels in the CNS of patients with sCJD, variant CJD (vCJD), iatrogenic CJD (iCJD), familial CJD (gCJD), fatal familial insomnia (FFI), Gerstmann-Sträussler-Scheinker (GSS), AD and age-matched controls. Our findings confirmed a striking and disease-specific up-regulation of SERPINA3 at both the mRNA and protein levels, across all types of human prion diseases. In contrast, only a mild upregulation was observed in the brain of AD patients (Vanni et al., 2017). These results prompted us to consider SERPINA3 as a potential biomarker for human prion diseases, representing a valid tool for distinguishing different forms of these disorders in humans. In mice, the clade A3 serpin gene is part of a cluster of fourteen genes (SerpinA3a-n). Notably, SerpinA3n shares 70 % homology with the human gene, making it the functional ortholog of human SERPINA3 in the brain (Forsyth et al., 2003; Horvath et al., 2004). SerpinA3n, like its human counterpart, is broadly distributed across multiple tissues. Several studies have reported an overexpression of SerpinA3n mRNA levels in different mouse models of prion disorders (Campbell et al., 1994; Dandoy-Dron et al., 2000; Xiang et al., 2004). We have also observed overexpression of SerpinA3n transcript and protein levels in the brains of outbred mice experimentally infected with RML (Vanni et al., 2017). In addition, we have demonstrated that by inhibiting the function of SerpinA3n, we could effectively reduce prion load in chronically infected cells (Colini Baldeschi et al., 2022). Considering that mice experimentally infected with prions mimic the changes in SerpinA3n that occur in the brain of prion-affected patients, we decided to thoroughly investigate the role of SerpinA3n in *ad hoc* generated animal models. In particular, we generated knock-out mouse models for SerpinA3n ($SerpinA3n^{-/-}$) and infected them with RML, 139A, or ME7 prion strains. The animals were closely monitored throughout the experiment. Neuropathological and biochemical analyses showed a lack of significant differences between $SerpinA3n^{-/-}$ and wild-type mice ($SerpinA3n^{+/+}$), regardless of the prion strain tested. However, we observed a notable dysregulation of other serpins in the brains of infected mice, suggesting the activation of a compensatory mechanism that comes into play during disease progression. These findings underscore the complexity of serpin interactions in prion pathogenesis and imply that alterations in serpin expression may be a broader phenomenon relevant to various NDs, including AD. This highlights the potential of targeting serpin pathways for therapeutic interventions in these conditions.

2. Results

2.1. Molecular characterization of $SerpinA3n^{-/-}$ mice

The modification of Serpina3n sequence present in $SerpinA3n^{-/-}$ mice consisted in a deletion of 402 bp and an insertion of 8 bp (ACAGTGTA) in intron 3 at chromosome 12 positive strand position 104,411,059 bp (TAACTGAGGAGAAGGTGGAGTCTCTG in GRCm38) and ending after CTGTTCTGTCCTCAGCCTAAGGCC at position 104,411,460 bp in intron 4 (Supplementary Information 1A, B). This mutation resulted in the deletion of exon 3, an amino acidic change after residue 212 and early truncation one amino acid later. The genotype was determined by the presence of bands at different molecular weights depending on the length of wild-type and/or mutant allele: $SerpinA3n^{+/+}$ mice showed one band at 232 bp while $SerpinA3n^{-/-}$ mice showed one band at 488 bp (Fig. 1A).

To characterize $SerpinA3n^{-/-}$ animals, SerpinA3n transcript and protein levels were analyzed in mouse brain tissue. The transcript region amplified by the RT-qPCR primer pair partially recognized the deleted region in $SerpinA3n^{-/-}$ mice (Supplementary Information 1C). RT-qPCR results normalized to three reference genes (*Actb*, *Gapdh* and *Tubb3*) demonstrated a total depletion of SerpinA3n mRNA in $SerpinA3n^{-/-}$ mice when compared to wild type mice (Mann-Whitney test, $p = 0.0079$, Fig. 1B). To assess putative compensation mechanism due to the overexpression of other serpin genes, gene expression analysis of brain-expressed serpins was performed (Zattoni et al., 2022). The relative levels of brain expressed serpins did not significantly vary in $SerpinA3n^{-/-}$ compared to wild type mice, except for a mild and not statistically significant upregulation of SerpinI1 in the brain of $SerpinA3n^{-/-}$ mice (Mann-Whitney test, $p = 0.095$, Fig. 1C). To assess the absence of SerpinA3n at the protein level, Western blot (Wb) on $SerpinA3n^{+/+}$ and $SerpinA3n^{-/-}$ mouse brain homogenates (BHs) were performed. Remarkably, we have used an in-house produced and characterized monoclonal antibody against mouse SerpinA3n. Among the clones able to recognize recombinant SerpinA3n (~47 kDa) in Wb, only MoSerAn.14 clone revealed a distinct banding pattern between BHs of $SerpinA3n^{+/+}$ and $SerpinA3n^{-/-}$ mice (Supplementary Information 2). The more intense Wb band, present in the $SerpinA3n^{+/+}$ sample and corresponding to the glycosylated form of SerpinA3n (~66 kDa), was absent in $SerpinA3n^{-/-}$ BH (Supplementary Information 2, Fig. 1D). After PNGase F treatment, the band corresponding to the glycosylated form of SerpinA3n (~66 kDa) observed in the $SerpinA3n^{+/+}$ BH has been shifted to a lower molecular weight (~47 kDa, corresponding to the size of recombinant protein). No band shifting has been observed in $SerpinA3n^{-/-}$ BH, suggesting that the additional bands represent unspecific signals of the monoclonal antibody MoSerAn.14 (Supplementary Information 3). Densitometric analysis revealed a statistical significant reduction of the glycosylated SerpinA3n Wb signal in $SerpinA3n^{-/-}$ animals, when compared to wild type mice (Mann-Whitney test, $p = 0.0079$, Fig. 1E).

2.2. The lack of SerpinA3n did not impact prion amplification by protein misfolding cyclic amplification (PMCA)

The efficiency of PMCA was not affected by the genetic background of the substrates ($SerpinA3n^{-/-}$ or $SerpinA3n^{+/+}$) and all prion strains

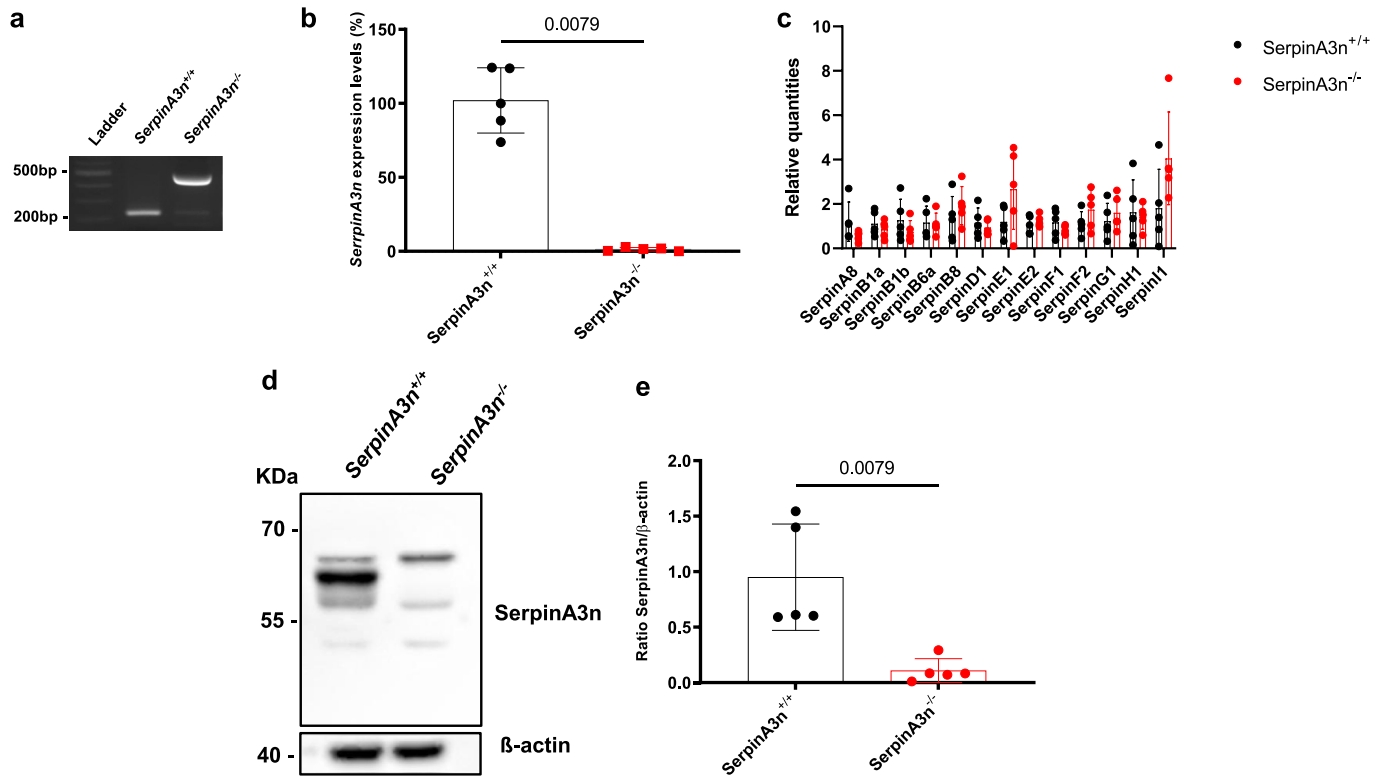

Fig. 1. Molecular characterization of SerpinA3n$^{-/-}$ mice. Agarose gel of PCR products from tail biopsy of SerpinA3n$^{+/+}$ and SerpinA3n$^{-/-}$ mice. DNA base pair lengths were shown on the left (bp) (A). RT-qPCR analysis for SerpinA3n mRNA expression in SerpinA3n$^{+/+}$ (n = 5) and SerpinA3n$^{-/-}$ (n = 5) mouse brain samples normalized to *Actb*, *Tubb3* and *Gapdh* as reference genes. The relative expression ratio was represented as percentage of expression compared to wild type animals. Statistical analysis was performed with Mann-Whitney test, *p* value = 0.0079 (B) RT-qPCR analysis for serpin mRNA expression in SerpinA3n$^{+/+}$ (n = 5) and SerpinA3n$^{-/-}$ (n = 5) mouse brain samples normalized to *Actb*, *Tubb3* and *Gapdh,* as reference genes. The relative expression ratio was represented as relative quantities of expression levels compared to wild type animals. Statistical analysis was performed with Mann-Whitney test (C). Representative Wb image of brain expressed SerpinA3n on SerpinA3n$^{+/+}$ and SerpinA3n$^{-/-}$ samples. β-actin was used as protein loading control and it was developed on the same membrane of SerpinA3n. Wb image has been cropped to improve clarity of the signal. Molecular weight was represented on the left (kDa) (**D**). Densitometric analysis of Wb of brain expressed SerpinA3n levels normalized on β-actin in SerpinA3n$^{+/+}$ (n = 5) and SerpinA3n$^{-/-}$ (n = 5). Statistical analysis was performed with Mann-Whitney test, *p* value = 0.0079 (**E**).

(RML, 139, and ME7) and dilutions were successfully amplified after a single round of amplification (Fig. 2A, B and C). The biochemical profiles of the amplified prions were all characterized by an equal representation of the di- and monoglycosylated bands. Interestingly, the ME7 amplified species showed an additional PrP band migrating just above the unglycosylated one (Fig. 2C). This unusual profile was observed using both substrates (SerpinA3n$^{-/-}$ and SerpinA3n$^{+/+}$ BHs), suggesting that it is likely an artifact of the PMCA process itself, rather than a biological difference due to the presence or absence of SerpinA3n. Thus, the lack of SerpinA3n did not show any evident effect in interfering with or promoting prion propagation *in vitro*. As expected, no prions were amplified in uninfected (mock) diluted substrates (Fig. 2D).

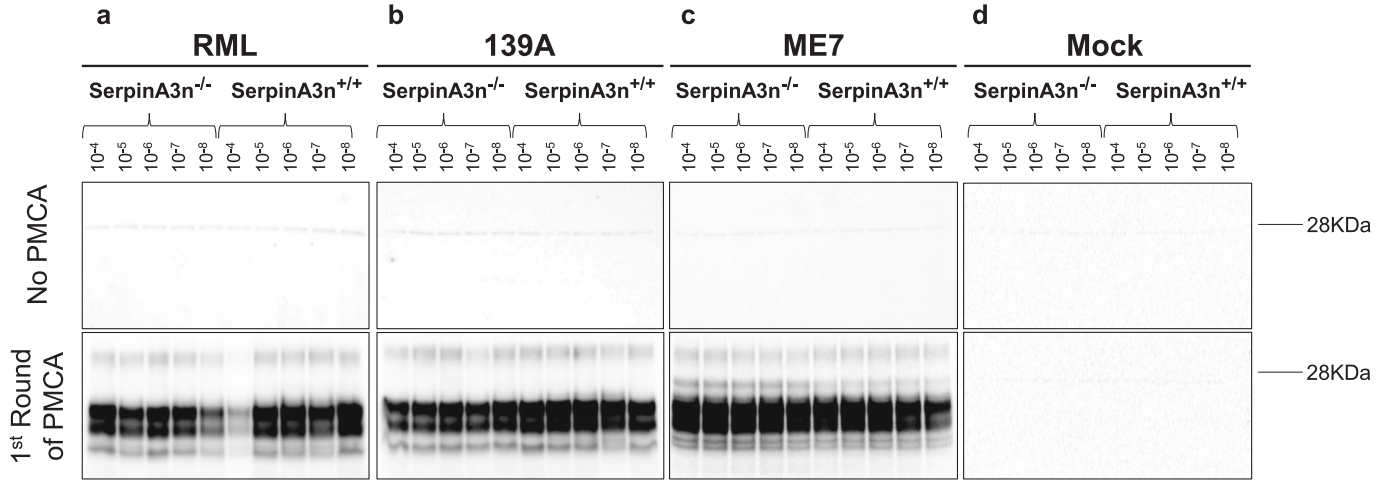

Fig. 2. PMCA analysis of prions. The results show that RML (**A**), 139A (**B**) and ME7 (**C**) can efficiently amplify in both SerpinA3n$^{-/-}$ or SerpinA3n$^{+/+}$ BHs. No amplification was observed in mock diluted samples (**D**).

2.3. All prion strains efficiently propagated in SerpinA3n$^{-/-}$ mice

To evaluate the potential involvement of SerpinA3n in the onset and progression of prion disease *in vivo*, SerpinA3n$^{-/-}$ and SerpinA3n$^{+/+}$ mice were inoculated with one of the following prion strains: RML, 139A, ME7. Animals inoculated with mock were used as a negative control. Regardless of genetic background, all prion-infected animals developed pathology, with incubation (IT) and survival (ST) times characteristic of each prion strain (Table 1 and Fig. 3). Importantly, one animal in group C and two in group F were withdrawn from the study due to non–prion-related health complications. No statistically significant differences in IT (RML $p = 0.0554$, 139A $p = 0.5775$, ME7 $p = 0.6240$) and ST (RML $p = 0.6392$, 139A $p = 0.7667$, ME7 $p = 0.6757$) were observed between SerpinA3n$^{-/-}$ and SerpinA3n$^{+/+}$ mice inoculated with the same prion strain (Log-rank test). The clinical presentation of the disease was similar in all inoculated animals and was mainly characterized by typical prion signs and symptoms, including ataxia, hunched posture and generalized tremors.

2.4. The lack of SerpinA3n did not influence the pathological properties of tested prions

Neuropathological analysis revealed similar changes in the brains of SerpinA3n$^{-/-}$ and SerpinA3n$^{+/+}$ mice injected with the same prion strain. Especially in the case of RML and ME7, spongiform changes mainly affected the thalamus, hippocampus, septum and frontal cortex while dorsal medulla, cerebellum, and hypothalamus were less affected. Spongiform alterations in all 139A infected mice were less pronounced than that of the other groups, but still more prevalent in the thalamus, hippocampus, septum, and frontal cortex (Fig. 4A, B and Supplementary Information 4). Immunohistochemical analysis showed the typical pattern of proteinase K (PK) resistant PrP (PrP^{res}) accumulation for each prion strain. Synaptic and diffuse deposition was observed throughout the brains with strong immunoreaction detected in the hippocampus, thalamus, and frontal cortex (Fig. 4B and Supplementary Information 4). No PrP^{res} deposition was observed in the brains of mice injected with mock. These findings indicate that the lack of SerpinA3n does not impact the onset, progression and neuropathological properties of prion disease in injected animals.

2.5. The lack of SerpinA3n did not influence the biochemical properties of prions

Biochemical analysis confirmed the presence of PrP^{res} in the brains of all inoculated mice. Unlike the results observed with PMCA, the RML (Fig. 5A), 139A (Fig. 5B) and ME7 (Fig. 5C) prions formed in the brains of SerpinA3n$^{-/-}$ and SerpinA3n$^{+/+}$ mice retained their specific biochemical properties, including their characteristic glycoform ratios, which were consistent across both animal genotypes. As expected, the unglycosylated bands of all prion strains migrated at 21 kDa. Densitometric analysis of the PrP^{res} load confirmed the lack of statistically significant differences between SerpinA3n$^{-/-}$ and SerpinA3n$^{+/+}$ mice injected with RML ($p = 0.3457$), 139A ($p = 0.8057$) and ME7 ($p = 0.7715$) (Mann-Whitney test). This suggests that the lack of SerpinA3n did not significantly alter the biochemical properties and propagation efficiency of all challenged prions. No prions were detected in the brains of mice inoculated with mock (Fig. 5D).

Table 1
Survival and incubation times. Regardless of genotype, animals inoculated with the same prion strain showed comparable incubation (IT) and survival (ST) times (d.p.i), with no statistically significant differences.

Genetic background	Inoculum	IT (Mean ± S.D.)	ST (Mean ± S.D.)
SerpinA3n$^{-/-}$	RML	135.8 ± 8.37	168.40 ± 6.80
SerpinA3n$^{+/+}$		164.4 ± 32.61	182.20 ± 37.04
SerpinA3n$^{-/-}$	139A	187.5 ± 19.43	207.30 ± 9.91
SerpinA3n$^{+/+}$		192.40 ± 34.09	210.40 ± 37.21
SerpinA3n$^{-/-}$	ME7	190.20 ± 35.89	218.20 ± 46.98
SerpinA3n$^{+/+}$		189.70 ± 42.77	199.30 ± 40

2.6. The lack of SeprinA3n did not influence the PK resistance properties of tested prions

The BHs of SerpinA3n$^{-/-}$ and SerpinA3n$^{+/+}$ mice inoculated with RML (Fig. 6A), 139A (Fig. 6B) or ME7 (Fig. 6C). For each prion strain, no differences in PK resistance were observed (two-way ANOVA, $p > 0.05$). These findings further support the hypothesis that the lack of SerpinA3n did not significantly affect the resistance of the prions to PK digestion.

2.7. Serpins gene expression analysis

To assess whether compensatory mechanisms could explain the lack of significant difference between SerpinA3n$^{-/-}$ and SerpinA3n$^{+/+}$ mice upon prion-injection, we performed gene expression analysis of other serpins, including SerpinA3n as internal control (Mann-Whitney test, $p = 0.0079$, Fig. 7A and $p = 0.0159$, Fig. 7B). Due to the limited availability of RML material, we performed the analyses on the brains of animals inoculated with the other two prion strains: ME7 and 139A. As expected, SerpinA3n$^{-/-}$ did not show detectable levels of *SerpinA3n*. Interestingly, we found a statistically significant upregulation of *SerpinB1b* (Mann-Whitney test, $p = 0.0371$, Fig. 7A) and downregulation of *SerpinD1* (Mann-Whitney test, $p = 0.0079$, Fig. 7A) in the brain of SerpinA3n$^{-/-}$ mice infected with 139A compared to SerpinA3n$^{-/-}$ animals. Interestingly, *SerpinF2* was upregulated in the brain of SerpinA3n$^{-/-}$ mice infected with ME7 (Mann-Whitney test, $p = 0.0079$, Fig. 7B) compared to SerpinA3n$^{-/-}$ animals. Notably, *SerpinF2* and *SerpinD1* are both involved in fibrinolysis, suggesting a correlation between prion disease and fibrinolysis pathway in the CNS. Altered thrombosis and fibrinolysis have been already associated to other NDs, including AD (Ledesma et al., 2000; Cortes-Canteli et al., 2010; Constantinescu et al., 2017; Angelucci et al., 2022).

3. Discussion

In this study, we explored the role of SerpinA3n in prion disease onset and its associated pathological properties using a combination of *in vitro* and *in vivo* approaches. We first characterized the brains of SerpinA3n$^{-/-}$ animals, confirming that SerpinA3n transcript and protein levels are depleted. Furthermore, performing gene expression analysis of other brain expressed serpin transcripts, we did not appreciate any statistically significant variation between SerpinA3n$^{+/+}$ and SerpinA3n$^{-/-}$ animals, suggesting no compensatory mechanisms exerted by other members of the serpin superfamily in physiological conditions.

We employed the PMCA technique to investigate whether SerpinA3n deletion affects prion amplification efficiency. Our findings demonstrated that the absence of SerpinA3n had no impact, as all tested prion strains (RML, 139A, and ME7) were successfully amplified across dilutions after a single round of PMCA. Intriguingly, we observed altered biochemical properties in amplified prions compared to the originals, regardless of the genetic background of the PMCA substrates. Amplified prions showed a more balanced representation of diglycosylated and monoglycosylated bands, deviating from the monoglycosylated band predominance seen in the original strains. A unique double-banding pattern was also identified in nonglycosylated ME7 prions, further underscoring the complexity of PMCA-induced changes. Recognizing that PMCA might not properly mimic the effects of SerpinA3n on prion propagation, we transitioned to animal studies to examine the effect of SerpinA3n deletion using a more physiologically relevant setting. The study in animal models appears to confirm the findings from the PMCA studies, as it did not reveal significant differences between SerpinA3n$^{+/}$

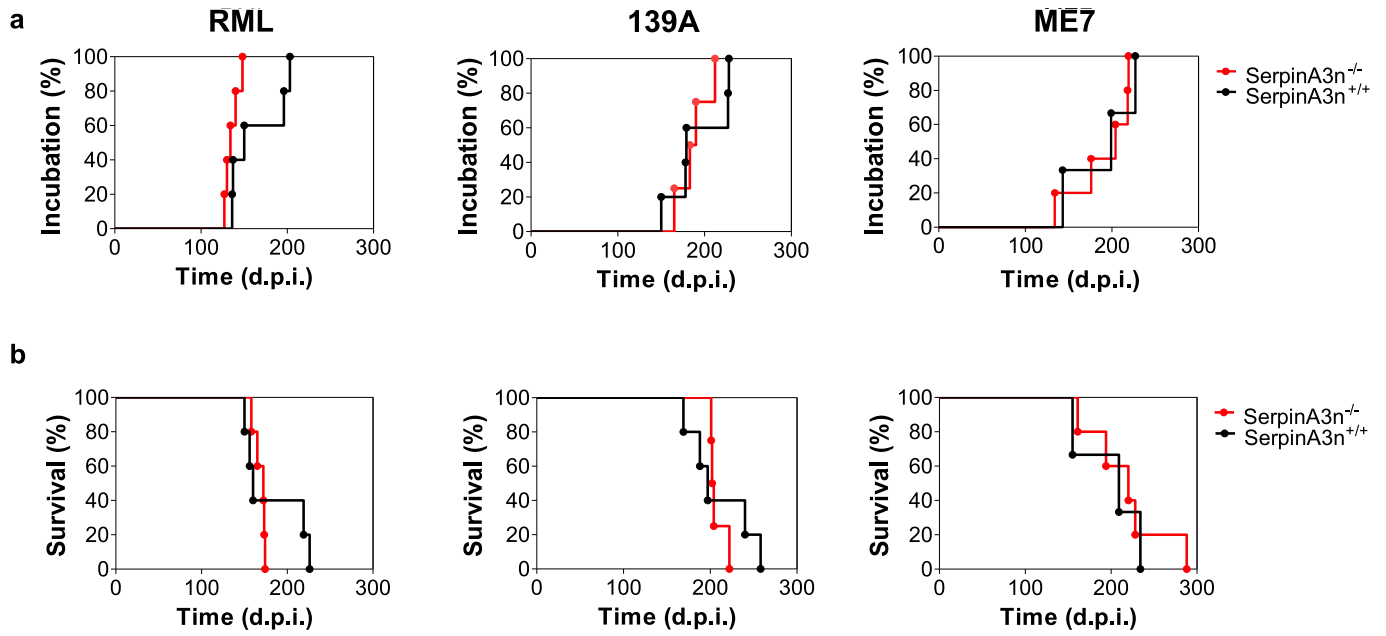

Fig. 3. Incubation and survival times of prion infected mice. The incubation (IT) (**A**) and survival (ST) (**B**) times were similar between SerpinA3n$^{-/-}$ (red lines) and SerpinA3n$^{+/+}$ (black lines) animals injected with the same prion strain: RML [SerpinA3n$^{-/-}$ (n = 5), SerpinA3n$^{+/+}$ (n = 5)], 139A [SerpinA3n$^{-/-}$ (n = 4), SerpinA3n$^{+/+}$ (n = 5)], and ME7 [SerpinA3n$^{-/-}$ (n = 5), SerpinA3n$^{+/+}$ (n = 3)]. (For interpretation of the references to color in this figure legend, the reader is referred to the web version of this article.)

$^{+}$ and SerpinA3n$^{-/-}$ mice inoculated with the prion strains, either in terms of incubation time, survival time, or neuropathological alterations. Marked spongiosis was observed in RML- and ME7-inoculated mice, predominantly in the hippocampus, septum, and cerebral cortex. While 139A-inoculated mice showed less pronounced spongiosis, prion deposition remained prominent across all groups. In particular, a diffuse synaptic deposition pattern of PrP^{res} was evident in the hippocampus, thalamus, and frontal cortex. Wb analysis of the CNS from both SerpinA3n$^{+/+}$ and SerpinA3n$^{-/-}$ mice revealed that the prions retained the biochemical properties of the original strains, notably showing a predominance of the mono-glycosylated band. Since no biochemical differences were observed, we subjected the samples to digestion with increasing concentrations of PK. This experiment aimed to assess whether, despite a similar glycoform ratio, the absence of SerpinA3n might have subtly influenced the biochemical properties of the prions. However, these analyses also failed to demonstrate any effect of SerpinA3n deficiency on the propagation, infectivity, or biochemical characteristics of the tested prions. It is worth noting that intracerebral prion inoculation might have masked any potential impact of SerpinA3n absence, as its role could be more critical and evident during the early stages of the disease. The direct introduction of a prion load into the brain likely initiated a severe neuropathological process, bypassing any initial regulatory influence SerpinA3n might have on prion propagation. Compared to the successful results published by our group in 2022 (Colini Baldeschi et al., 2022) showing that the pharmacological inhibition of SerpinA3n was able to clear prions from cells, PMCA and *in vivo* studies failed to support these findings. Certainly, the use of animal models introduced a more relevant physiological environment where a complex interplay between neurons, glial cells, and other components of the extracellular matrix might have overcome the effects of SerpinA3n deletion. In this regard, one of the most striking findings was the altered expression of other serpins in SerpinA3n$^{-/-}$, pointing to compensatory mechanisms that sustain prion propagation in the absence of this specific serpin. Interestingly, these changes appeared to be prion-strain specific, as 139A-inoculated mice displayed altered serpin profiles distinct from those of ME7-inoculated mice. While we lacked material to assess serpin levels in RML-inoculated mice, our prior studies indicate that both *SerpinA3n* and *SerpinF2* are significantly upregulated in RML-infected brains of CD1 mice, further supporting the notion of strain-specific serpin responses (Zattoni et al., 2022). Therefore, considering also the results obtained in a different experimental context, we cannot exclude the possibility that a prion-specific serpin alteration could occur. The compensatory upregulation of other serpin family members in the brains of prion-inoculated SerpinA3n$^{-/-}$ mice is an intriguing finding, suggesting that the CNS might activate alternative protective mechanisms in response to prion infection when SerpinA3n is absent. In the present study, the overexpression of *SerpinF2* may lead to higher degree of plasmin inactivation that would lead to a lower degree of fibrin and other extracellular proteins degradation. At the same time, the downregulation of *SerpinD1* leads to lower inhibition of thrombin that, as for the case of *SerpinF2* overexpression, would lead to higher degree of fibrin load, worsening protein clearance mechanisms. The compensatory mechanisms observed in the brains of SerpinA3n$^{-/-}$ mice highlight the capacity of CNS to adapt to prion infection by modulating serpins expression. Such findings have broader implications, suggesting that serpins are integral to protease regulation pathways in prion diseases and possibly other NDs caused by misfolded forms of α-synuclein, tau, β-amyloid, and TDP-43. In light of these potential compensatory mechanisms, it is worth considering the possibility of blocking not only SerpinA3n but a combination of several (if not all) serpins to assess whether disrupting the compensatory effect could interfere with prion propagation and potentially with the propagation of the other prion-like proteins. Furthermore, neuroinflammation, a hallmark of prion and other NDs, may be modulated by SerpinA3n, as this acute-phase protein responds to inflammatory cues and shapes the CNS microenvironment. SerpinA3n is upregulated in response to inflammatory signals which could influence the neuroinflammatory responses that drive prion propagation and the neurodegenerative cascade. Therefore, targeting SerpinA3n or related pathways could provide innovative therapeutic strategies, not only for prion diseases but also for conditions like Alzheimer's, Parkinson's, and amyotrophic lateral sclerosis, where neuroinflammation is not merely a consequence but an active participant in disease pathogenesis. Our findings strengthen the importance of investigating the role of SERPINA3/SerpinA3n in neurodegeneration,

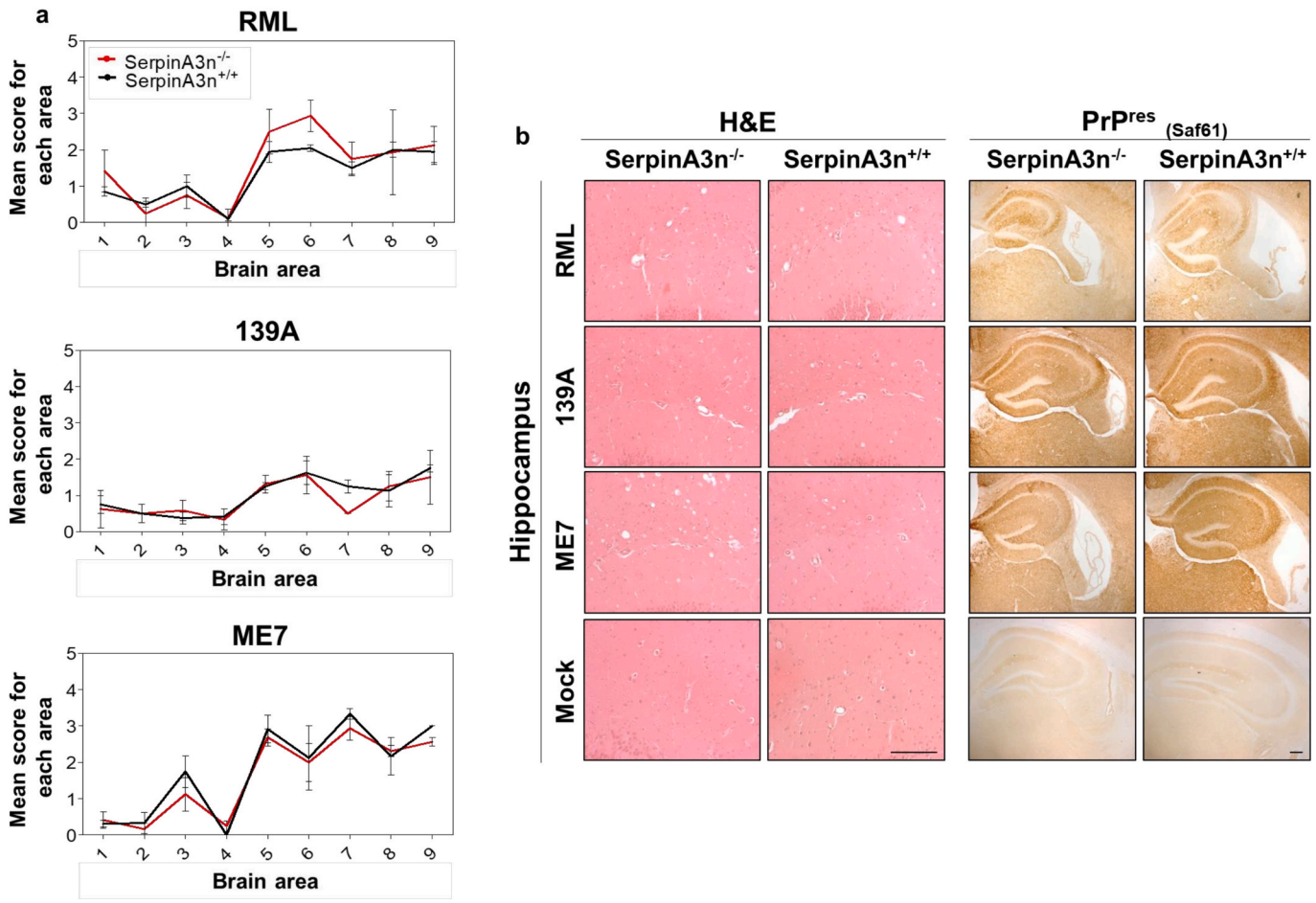

Fig. 4. Neuropathological analysis. Lesion profile of SerpinA3n$^{-/-}$ (red lines) and SerpinA3n$^{+/+}$ (black lines) mice injected with RML, 139A, or ME7 prion strains (**A**). The spongiform alterations were evaluated on hematoxylin and eosin stained sections (H&E) in nine standard brain areas: (1) dorsal medulla, (2) cerebellar cortex, (3) midbrain, (4) hypothalamus, (5) thalamus, (6) hippocampus, (7) septum, (8) retrosplenial and adjacent motor cortex, cingulated and (9) adjacent motor cortex. Error bars represent the standard deviation of the mean (mean ± SD). H&E and immunohistochemical analyses revealed pathological alterations characteristic of each prion strain, with no differences observed between SerpinA3n$^{-/-}$ and SerpinA3n$^{+/+}$ mice. No spongiosis and PrP^{res} were found in the brains of SerpinA3n$^{-/-}$ and SerpinA3n$^{+/+}$ mice inoculated with mock. Scale bar in H&E staining, 10 μm; scale bar in immunohistochemical staining, 30 μm (**B**). (For interpretation of the references to color in this figure legend, the reader is referred to the web version of this article).

particularly concerning how it may influence both the inflammation and the degradation of protein aggregates through protease-dependent pathways. Notably, the aggregation of pathological proteins in the brain starts much earlier than the onset of clinical symptoms. As the disease progresses, the cerebral protein clearance mechanisms may become unable to effectively eliminate these aggregates. Additionally, age-related increases in the expression of protease inhibitors like SERPINA3 may contribute to the saturation of these clearance systems, impairing the protease-driven degradation of aggregated proteins. This failure ultimately results in significant brain damage and the emergence of clinical symptoms. This highlights a critical intersection between neurodegeneration, inflammation, aging, and protease activities, underscoring the potential therapeutic value of targeting serpins to restore proper protein homeostasis. These findings broaden the understanding of serpin family proteins as potential therapeutic targets, emphasizing their compensatory and regulatory roles in maintaining protein homeostasis and controlling brain inflammation. However, identifying SERPINA3/SerpinA3n functions in the CNS is very challenging, due to their intrinsic metastability, the high number of paralogs and their lower expression in physiological conditions (Heit et al., 2013). Future investigations should focus on dissecting these mechanisms to develop innovative treatments for prion diseases and other NDs driven by prion-like proteins.

4. Materials and methods

4.1. Ethics statement

C57BL/6N-Serpina3nem1(IMPC)J/Mmucd mice were purchased from Davis University of California. Animals were housed in individually ventilated cages (2–3 mice per cage), fed and provided with water. Lighting was on an automatic 12 h basis. The animal facility is licensed and inspected by the Italian Ministry of Health. Current animal husbandry and housing practices comply with the Council of Europe Convention ETS123 (European Convention for the Protection of Vertebrate Animals used for Experimental and Other Scientific Purposes; Strasbourg, 18.03.1986), Italian Legislative Decree 116/92 (Gazzetta Ufficiale della Repubblica Italiana, 18th February 1992), and with the 86/609/EEC (Council Directive of 24 November 1986 on the approximation of laws, regulations, and administrative provisions of the Member States regarding the protection of animals used for experimental and other scientific purposes). The study, including its ethical aspects, was approved by the Italian Ministry of Health (Permit Number: 641/2020-PR), and all efforts were made to minimize animal suffering.

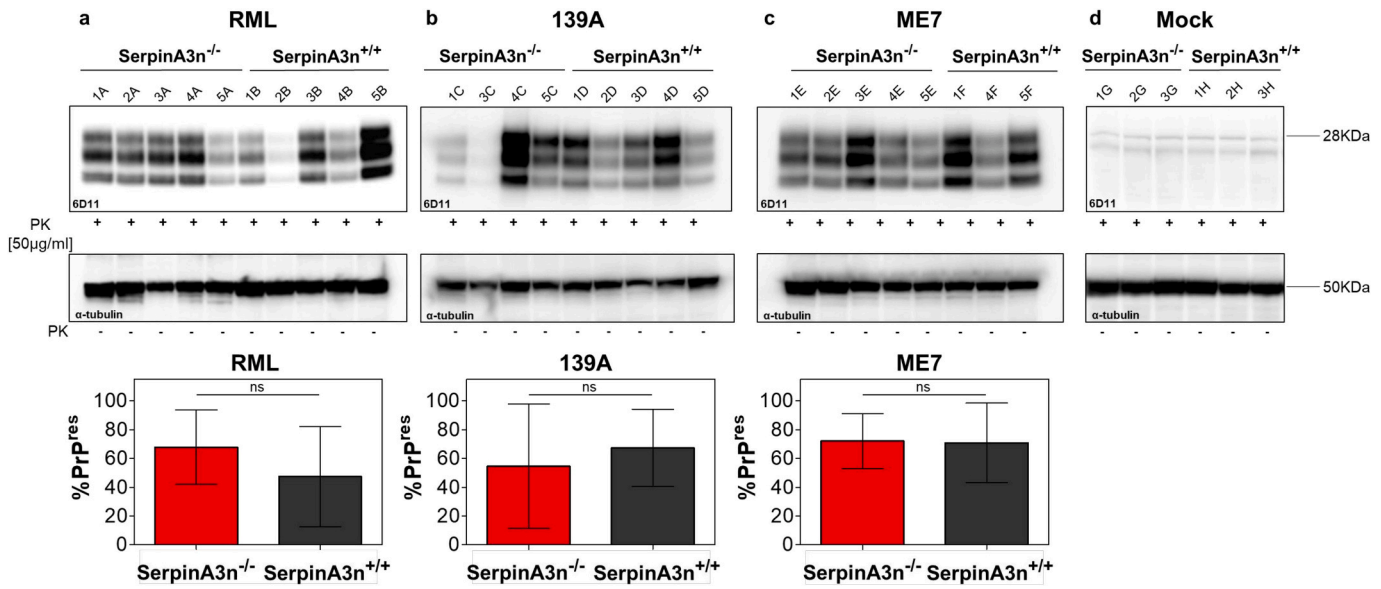

Fig. 5. Biochemical analysis of brains from prion-infected mice. After proteinase K (PK) digestion, comparable levels of RML were detected in the brains of both SerpinA3n$^{-/-}$ and SerpinA3n$^{+/+}$ inoculated mice (**A**). Each lane on the Western blot corresponds to the content of PrP^{res} present in the brain of every animal. The number codes assigned to each lane served as relative identifiers for the animals. Likewise, similar levels of 139A (**B**) and ME7 (**C**) prions were observed in the brains of SerpinA3n$^{-/-}$ and SerpinA3n$^{+/+}$ mice. Densitometric analysis confirmed that the differences in total PrP^{res} load between SerpinA3n$^{-/-}$ (red histograms) and SerpinA3n$^{+/+}$ (black histograms) animals are not statistically significant (ns), regardless of the inoculum. No prions were detected in the brains of both SerpinA3n$^{-/-}$ and SerpinA3n$^{+/+}$ mice inoculated with mock (**D**). (For interpretation of the references to color in this figure legend, the reader is referred to the web version of this article.)

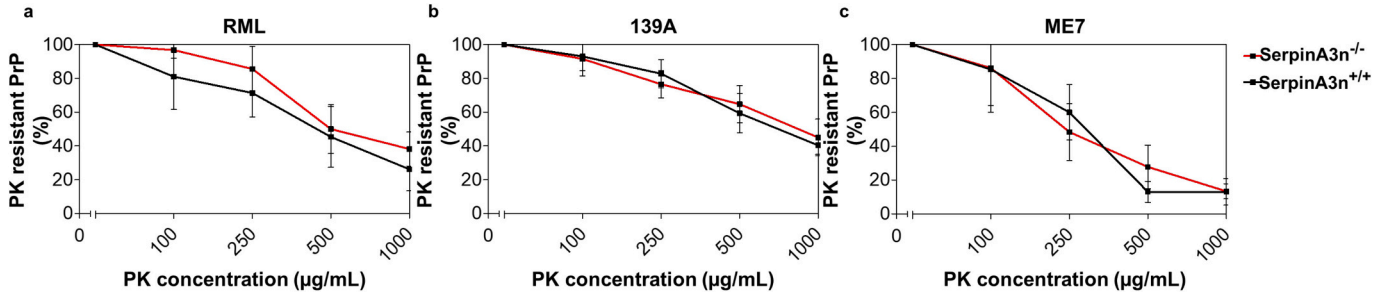

Fig. 6. PK resistance assay. Comparable resistance to different concentrations of PK (50, 100, 250, 500, and 1000 μg/mL) was detected in the brains of both SerpinA3n$^{-/-}$ and SerpinA3n$^{+/+}$ mice injected with RML (**A**) 139A (**B**) or ME7 (**C**). Densitometric analysis of PrP^{res} signals confirmed the lack of statistically significant differences between groups of animals.

4.2. Generation of SerpinA3n knockout (C57BL/6N-Serpina3nem1 (IMPC)J) mice

SerpinA3n knockout (C57BL/6N-Serpina3n$^{em1(IMPC)J}$, SerpinA3n$^{-/-}$) mice were obtained from the Mutant Mouse Resource and Research Center (MMRRC), University of California, Davis (USA). RNA guides (recognizing CTCAGAAGCGGTGTTAACTG, AGTGCCCATGATGAGCATGG and CCTGTTCTGTCCTCAGCCTA sequences) and Cas9 were microinjected into C57BL/N6 zygotes. DNA for genotyping was extracted from 0.2 to 0.5 cm tail or ear biopsies, with the following protocols. Tail snips were digested in 250 μL tail buffer (100 mM Tris pH 8.5, 5 mM EDTA pH 8.0, 125 mM NaCl, 0.2 % SDS) and 100 μg/mL proteinase K (#EMR022001, Euroclone), and then placed in shaker at 55 °C at 500 rpm overnight. The samples were centrifuged for 5 min at room temperature at maximum speed. The supernatant was collected and 300 μL of EtOH 100 % were added. The samples were centrifuged for 5 min at room temperature at maximum speed and supernatant was discarded. 600 μL of EtOH 70 % were added to the pellet and were centrifuged at maximum speed for 5 min. The supernatant was removed, and the step was repeated. The pellet was let dry and 100 μL of TE Buffer was added. The samples were heated for 30 min at 56 °C and then vortexed. For the "HotSHOT" DNA purification protocol (Truett et al., 2000), performed on ear biopsies, 75 μL of 15 mM NaOH, 0.2 mM disodium EDTA pH 12.0 were added to the samples. They were then placed in Veriti™ 96-well Thermo Cycler (Applied Biosystems) at 98 °C for 1 h. Seventy-five μL of Tris HCl pH 5.5, were then added, and the samples were centrifuged at 800*g* for 5 min. A 1:10 dilution of stock sample, from tail or ear biopsies, was used as template for subsequent PCR reactions, carried out in 12 μL on 96-well plates using KAPA2G Fast HotStart PCR Kit (#KK5510, Sigma-Aldrich). Primers were designed by The Jackson Laboratory as follows in Table 2.

PCR cycling program on a Veriti™ 96-well Thermo Cycler (Applied Biosystems) was the following: 94 °C for 2 min; 94 °C for 20 s, 65 °C for 15 s, 68 °C for 10 s for 10 cycles; 94 °C for 15 s; 60 °C for 15 s; 72 °C for 10 s for 28 cycles; 72 °C for 2 min; 10 °C. PCR products were loaded on 2 % agarose gel in TBE 0.5×, containing Midori Green Advance (# MG04, NIPPON Genetics) (1:15000), at a fixed voltage (90–110 V) and then visualized at transilluminator. Brains from six-month-old SerpinA3n$^{-/-}$ (n = 5) and SerpinA3n$^{+/+}$ (n = 5) were used to confirm SerpinA3n transcript and protein ablation expression.

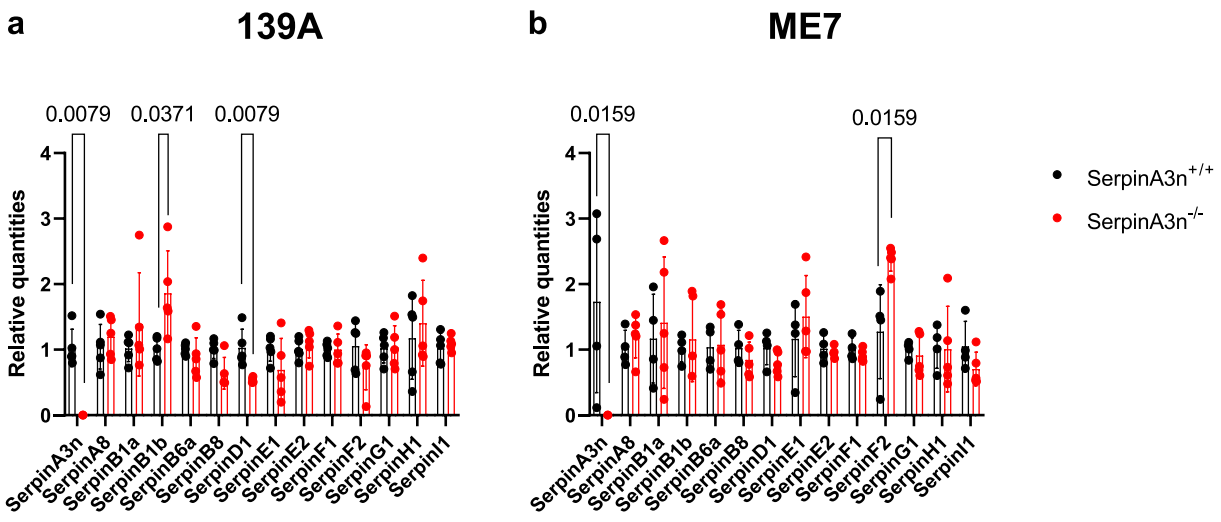

Fig. 7. Serpins expression level in SerpinA3n$^{-/-}$ and SerpinA3n$^{+/+}$ mice injected with prions. RT-qPCR analysis was performed to evaluate serpins mRNA expression in mouse brain samples from 139A (**A**) and ME7 (**B**) prion-injected SerpinA3n$^{+/+}$ (n = 4 for both 139A and ME7) and SerpinA3n$^{-/-}$ (n = 5 for 139A, n = 4 for ME7) groups. Higher levels of *SerpinB1b* and lower levels of *SerpinD1* were found in the brain of SerpinA3n$^{-/-}$ mice injected with 139 compared to inoculated SerpinA3n$^{+/+}$ animals. Higher levels of *SerpinF2* were found in the brain of SerpinA3n$^{-/-}$ mice injected with ME7 compared to injected SerpinA3n$^{+/+}$ animals. Expression levels were normalized against reference genes *Actb, Tubb3,* and *Gapdh.* The relative expression ratios were calculated as quantities relative to those in SerpinA3n$^{+/+}$ animals. Statistical significance was assessed using the Mann-Whitney test.

Table 2
Primer sequences for PCR analysis.

Name	Primer sequence 5′ ➔ 3′
Common	AAC CAA GCC TGG AGA CAA TG
Wild-type reverse	CGT GTC AAG AGG GTC AAA GG
Mutant reverse	TTA AGT CAG AGC CTG GCA CA

4.3. Preparation of the substrate for PMCA analysis

The brains of SerpinA3n$^{-/-}$ and SerpinA3n$^{+/+}$ mice were homogenized at 10 % (*w/v*) in conversion buffer (150 mM NaCl, 1 % Triton X-100 in PBS), supplemented with a complete protease inhibitor cocktail (Roche), and used as PMCA substrates.

4.4. Preparation of the inocula for PMCA analysis or mouse bioassay

Ten percent (weight/volume, w/v) brain homogenates (BHs) of mice infected with RML, 139A, ME7 or uninfected (mock) were prepared in sterile PBS and used for the PMCA or the inoculation.

4.5. PMCA analysis of prion strains

Inocula were serially diluted (from 10^{-3} to 10^{-7}, volume/volume, v/v) in 10 % control BHs. Ten µL of each dilution was added to 90 µL of PMCA substrate (BHs of either SerpinA3n$^{-/-}$ or SerpinA3n$^{+/+}$ mice), transferred into 0.2 mL PCR tubes, and subjected to amplification using a Qsonica Q700 sonicator. PMCA consisted of intermittent cycles of incubation (29 min and 40 s) and sonication (20 s set at 250–270 W). After 48 h of reaction (considered as a round of amplification), 10 µL of the amplified material was added to 90 µL of freshly prepared PMCA substrate and an additional round of amplification was performed. In total, each sample was subjected to two PMCA rounds.

4.6. Proteinase-K digestion of PMCA-generated products

Ten µL of PMCA-generated products were treated with 100 µg/mL of proteinase K (PK, Invitrogen) for 1 h at 37 °C under shaking (550 rpm) before Western blot (Wb) analysis and immunoblotting with 6D11 antibody (1:5000, epitopes 93–109, Covance).

4.7. Intracerebral injection of RML,139A, ME7 or mock brain homogenates

All surgical procedures were performed under sterile conditions at Fondazione IRCCS Istituto Neurologico Carlo Besta. Three-month-old SerpinA3n$^{-/-}$ and SerpinA3n$^{+/+}$ mice were anesthetized with Tiletamine-Zolazepam (10 mg/Kg) and stereotaxically injected with a specific inoculum in the right hippocampus with 2.5 µL, as summarized in Table 3. Each group consisted of 5 animals, except for the mock-inoculated group, in which 3 animals were used.

4.8. Incubation and survival time

The incubation time (IT) was calculated considering the time between RML, 139A, or ME7 inoculation and symptoms onset, including ataxia (uncoordinated movements), tail rigidity, and kyphosis (hunched back). Survival time (ST) was calculated as the time between prions injection and the sacrifice of the animals. Brains were then harvested, and the right hemisphere was used for neuropathological assessments while the left one was used for RNA extraction and other biochemical analyses (see Fig. 8. Graphic representation below).

4.9. RNA isolation

Once harvested, part of the left brain hemisphere was homogenized using T 10 basic ULTRA-TURRAX® homogenizer (# 0003737000, IKA

Table 3
Summary of the experimental groups included in the study.

Group code	Animal genotype	Number of animals	Injected material
A	SerpinA3n$^{-/-}$	5	RML
B	SerpinA3n$^{+/+}$	5	
C	SerpinA3n$^{-/-}$	5[a]	139A
D	SerpinA3n$^{+/+}$	5	
E	SerpinA3n$^{-/-}$	5	ME7
F	SerpinA3n$^{+/+}$	5[a]	
G	SerpinA3n$^{-/-}$	3	mock
H	SerpinA3n$^{+/+}$	3	

[a] One animal in group C and two in group F were withdrawn from the study due to non–prion-related health complications.

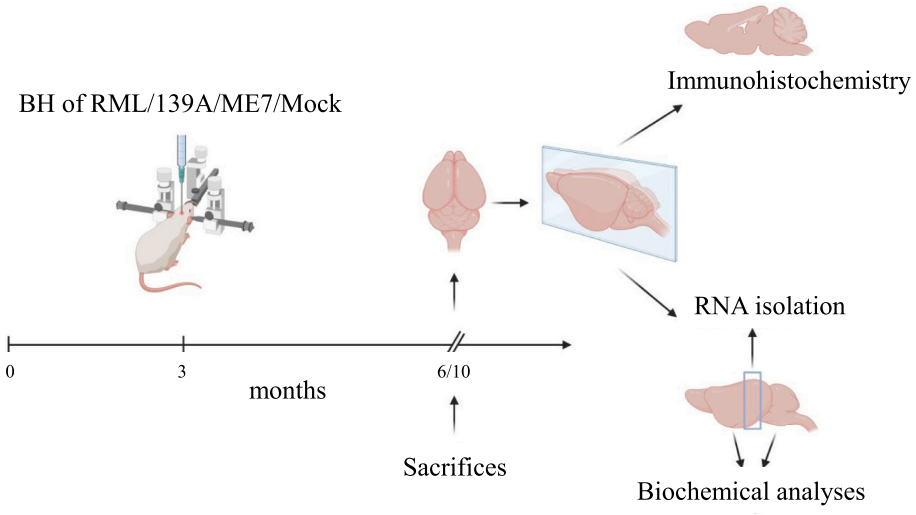

Fig. 8. Graphic representation of the experimental design: Three-month-old SerpinA3n$^{-/-}$ or SerpinA3n$^{+/+}$ mice were stereotaxically injected with either RML, 139A, ME7 or mock brain homogenates (BHs). Symptomatic animals were sacrificed and the brains were divided into two halves. The left hemisphere was used for RNA and biochemical analyses, while the right hemisphere was used for neuropathological evaluations (*image created with Biorender.com*).

Dispersers) in 1 mL TRIzol™ Reagent (# 15596026, Invitrogen). RNA was extracted with PureLink® RNA Mini Kit (#12183020, Life Technologies) and on-column DNA digestion was performed using PureLink® DNase Set (# 12185010 Life Technologies). RNA was checked for concentration and purity on DS-11 Spectrophotometer (DeNovix). RNA integrity was analyzed using 2100 Bioanalyzer (# G2939BA, Agilent Technologies) with an RNA Integrity Number ≥ 8, or determined by agarose gel (1 %) analysis, presenting sharp 28S and 18S rRNA bands.

4.10. Quantitative reverse transcription polymerase chain reaction (RT-qPCR)

cDNA was obtained starting from 1 μg of total RNA with 50 μM Oligo (dT)20 (#AM5730G, Invitrogen), 10 mM ea dNTP mix (#18427013, Invitrogen), 40 U RNaseOUT™ Recombinant Ribonuclease Inhibitor (#10777019, Invitrogen), 5× First Strand Buffer, 0.1 M DTT and 200 U SuperScript® III Reverse Transcriptase (#18080093, Invitrogen). A negative control was performed for each sample by omitting the reverse transcriptase. qPCR primers were designed as previously described (Zattoni et al., 2022) (Table 4).

Gene expression assays were performed using iQTM SYBR® Green Supermix 2× (170–8882, Bio-Rad Laboratories), 400 nM final concentration of the corresponding forward and reverse primer (Sigma-Aldrich) and 10 ng/μL final concentration of cDNA samples. CFX96 Real-Time System C1000 Touch™ Thermal Cycler (Bio-Rad Laboratories) was used to perform amplification and cycling conditions, including an initial denaturation of 3 min at 95 °C, the 45 cycles at 95 °C for 10 s, and 60 °C for 1 min. qPCR reaction was performed in 96-well plates, performing duplicates for each primer pair and sample. No reverse transcriptase control for each primer pair was analyzed to evaluate possible genomic DNA contamination and no template control was added in each plate to exclude the presence of contaminating DNA in the qPCR reaction mix. Melting curve analysis of each amplicon was performed for each primer pair to verify that artificial products or primer dimers were not responsible for the fluorescence signal obtained. Differential expression of target genes was normalized to three different reference genes (*Actb*, *Gapdh* and *Tubb3*) expression, considering that the expression stability of these three housekeeping genes was previously assessed (Vanni et al., 2017; Zattoni et al., 2022). The absolute expression value (C_T) of each serpin gene was addressed in mouse brain pool to select genes having a $C_T \leq 35$ (Vanni et al., 2018). The relative expression ratio (fold change) was calculated using an adapted version of $2^{-\Delta\Delta CT}$ method (Livak and Schmittgen, 2001). ΔC_{Ts} of each sample were calculated subtracting the average C_T of the three housekeeping

Table 4
Primer sequences for RT-qPCR analysis.

Gene	Forward primer sequence 5′ → 3′	Reverse primer sequence 5′ → 3′
Gapdh	TTCACCACCATGGAGAAGGC	GGCATGGACTGTGGTCATGA
Tubb3	CGCCTTTGGACACCTATTC	TACTCCTCACGCACCTTG
Actb	CACACCCGCCACCAGTTC	CACACCCGCCACCAGTTC
SerpinA3n	ACCCTGAGGAAGTGGAAGAA	CCTGATGCCCAGCTTTGAAA
SerpinA8	TGTCTAGGTTGGCGCTGAAG	GATGTATACGCGGTCCCCAG
SerpinB1a	GTTTTCCTCCTCGGCTTTTGC	AGTTTGAGGATGGAGTCGTCC
SerpinB1b	GTGCTTGCCAGTAAGACACTC	ATGGTGAAGGCTCCTCTGTAG
SerpinB6a	TTCCTGCACCCTTCTGTGTC	TGAAGCCGCCTAGATTCTCC
SerpinB8	TCGTGTGATTTCCTTTCGACCT	TTCCTGCACCCTTCTGTGTC
SerpinD1	GAATGGCAATATGTCAGGCATC	CACTGTGATGGTACTTTGGTGCTT
SerpinE1	TCCACAAGTCTGATGGCAGC	GGGGTGGTGAACTCAGTGTA
SerpinE2	CACATGGGATCGCGTCCATC	CAGCACTTTACCAACTCCGTTTA
SerpinF1	ACGATCTGTACCGCCTGAGA	TTCGATGTTCAGCTCCCAGAG
SerpinF2	TTCTCCTCAACGCCATCCA	GGTGAGGCTCGGGTCAAAC
SerpinG1	GAACTTGGACCAGGACGCAG	GCTGGTAGCTTCGGGATCTG
SerpinH1	CCGGCCCAGAATGAAAAAGGC	TAAGGTGCCCAGAAGGAGAGA
SerpinI1	CGCCATTCAATGGGATATG	CAAAGAGCGAATTGGCAAG

gene to the C_T of the target one, both for "test" (prion-infected SerpinA3n$^{-/-}$ and SerpinA3n$^{+/+}$ mice) and "calibrator" (not-infected control SerpinA3n$^{-/-}$ and SerpinA3n$^{+/+}$ mice, respectively). Then, $\Delta\Delta C_T$ were obtained with the ΔC_T of each sample (of both test and calibrator) minus the average ΔC_T of the calibrator samples (not-infected SerpinA3n$^{+/+}$ or SerpinA3n$^{-/-}$ mice, respectively). Fold change (FC) values smaller than 1 were converted using the equation $-1/FC$, for representation. For an ease representation, FC of SerpinA3n transcript was transformed into percentage of expression.

4.11. Biochemical analysis for SerpinA3n

The other part of the left brain hemisphere from SerpinA3n$^{-/-}$ and SerpinA3n$^{+/+}$ mice was homogenized at 10 % (*w/v*) in lysis buffer (10 mM Tris–HCl pH 8.0, 150 mM NaCl, 0.5 % NP40, 0.5 % deoxycholic acid sodium salt). Samples were centrifuged for 1 min at 4 °C, at 800*g*. Protein concentration of cleared homogenates was determined by Bicinchoninic Acid (BCA) method using the bicinchoninic acid solution (#B9643, Sigma-Aldrich) and Copper(II) sulphate solution (#C2284, Sigma-Aldrich) in 1:50 dilution, and protein standard (#P0834, Sigma-Aldrich) to build the standard curve. After 30 min at 37 °C the reaction was visualized on Enspire Multimode Plate Reader (PerkinElmer). The desired amount of proteins was loaded onto 9 % or 12 % Acrylamide/Bis-acrylamide (#A7802 Sigma-Aldrich) gels, for SerpinA3n detection respectively, and separated by SDS-PAGE using SE 600 Ruby (GE Healthcare). SerpinA3n recombinant protein, produced as previously described (Zattoni et al., 2022; Colini Baldeschi et al., 2022), was used as molecular weight marker control. Gels were then transferred to PVDF membrane (Millipore) using Criterion Blotter (Bio-Rad) for 2 h at 4 °C. After 1 h of blocking in 5 % milk in TBS-T, membranes were incubated with monoclonal anti-mouse SerpinA3n antibody (MoSerA3n.14, 1 μg/mL). The following day, after three washes in TBS-T, membranes were incubated for one hour with rabbit anti-goat horseradish peroxidase (HRP) secondary antibody for SerpinA3n detection and, subsequently, monoclonal anti-β-actin−peroxidase antibody (1:10,000, Sigma-Aldrich) or β-tubulin antibody (Sigma-Aldrich). After three washes of the membranes with TBS-T, the reactions were visualized by chemiluminescence on UVITEC (Cambridge) using Immobilon Classico Western HRP substrate (#WBLUC0500, Millipore). Densitometric analysis was carried out using UVIBand software.

4.12. Biochemical analysis for prion detection

The parts of the left hemisphere that were not used for RNA analysis, were homogenized at 10 % (*w/v*) in lysis buffer composed of 100 mM NaCl, 10 mM EDTA, 0.5 % NP40, 0.5 % sodium deoxycholate and 10 mM Tris-HCl pH 7.4. After a preliminary centrifugation (800*g*, 1 min) 10 μL of BHs were treated with 50 μg/mL of PK (1 h, 37 °C, 550 rpm, Invitrogen). PK digestion was stopped by boiling the samples in loading buffer (Bolt LDS Sample Buffer and DTT, ThermoScientific) at 100 °C for 10 min. The electrophoretic separation was done by using 12 % Bis-Tris plus gels (ThermoScientific) and the proteins were transferred into polyvinylidene difluoride membranes (PVDF, Millipore). After blocking with non-fat dry milk (1 h at room temperature), the membranes were probed with the monoclonal anti-PrP antibody 6D11 (1:5,000) (which recognizes the N-terminal part of the PrP [a.a. 93–109]; 0.2 μg/mL – Covance SIG-399810) over-night at 4 °C. After incubation with secondary antibody (Fab fragment anti-mouse IgG conjugated with HRP, GE), membranes were developed using the ECL Prime detection system (Amersham) and chemiluminescence was visualized using a G:BOX Chemi Syngene system. Ten μL of BH was not treated with PK and probed with the monoclonal anti α-tubulin antibody (1:10,000, Sigma) to normalize the biochemical signal.

4.13. PK-resistance assay

BHs were initially centrifuged (800*g*, 1 min). Ten μL of each BHs were treated with five increasing concentrations of PK (50, 100, 250, 500, and 1,000 μg/mL) and incubated for 1 h at 37 °C under shaking (550 rpm). The enzymatic activity was stopped by boiling the samples in loading buffer (Bolt LDS Sample Buffer and DTT, ThermoScientific) at 100 °C for 10 min. Samples were subjected to Wb analyses and membranes were immunoblotted with the 6D11 antibody (1:5,000). Resulting PK-resistant PrP (PrP^{res}) bands were subjected to densitometric quantification analyses using the ImageJ software.

4.14. Neuropathological analysis

The right hemispheres of the brain were fixed in FineFix, dehydrated and embedded in paraffin (Bio-Optica). Seven μm-thick serial sections were cut and stained with hematoxylin and eosin (H&E) or immunostained with monoclonal antibody to PrP (Saf61 1:400, Alfatech Advanced lab solutions). Lesion severity was scored on hematoxylin and eosin (H&E)-stained coronal brain sections using a semi-quantitative scale from 0 (no vacuolation) to 5 (severe vacuolation) described by Fraser et al. (Fraser and Dickinson, 1968). Scoring was performed in nine brain regions classically affected in prion disease: (1) dorsal medulla, (2) cerebellar cortex, (3) midbrain, (4) hypothalamus, (5) thalamus, (6) hippocampus, (7) septum, (8) retrosplenial and adjacent cingulate cortex, and (9) adjacent motor cortex. Before PrP immunostaining, the sections were treated with 10 μg/mL PK (Invitrogen) for 5 min at room temperature and 3 M guanidine isothiocyanate (Merck) for 20 min at room temperature. Unspecific binding of the secondary antibody was prevented using the animal research kit (ARK, Dako). Immunoreactions were visualized using 3–3′-diaminobenzidine (DAB, Dako) as a substrate-chromogen system. Lesion profiles were performed on H&E stained sections, as previously described (Fraser and Dickinson, 1967). All images were acquired with Nikon Eclipse E800 microscope equipped with Nikon digital camera DXM 1200 and Nikon ACT-1 (v2.63) acquisition software.

4.15. Statistical analysis

Data were processed and analyzed using Prism software (v5.0 GraphPad, Boston, MA, USA). Kaplan-Meier survival curves were plotted and differences in incubation and survival times between groups of animals were compared using the Logrank test. Different groups were assessed by two-way analysis of variance (ANOVA) for multiple comparisons followed by Bonferroni's *post hoc* test. Unpaired *t*-test, two-tailed, was also used for the *p*-value calculation. Mean values are presented with their standard deviations of the mean (S.D.). Non-parametric Mann–Whitney *U* test was used to compare lesion scores between SerpinA3n$^{-}/^{-}$ and SerpinA3n$^{+}/^{+}$ mice inoculated with the same prion strain. The densitometric analysis of Wb bands was performed using ImageJ software (1.51v). Graphic representations of densitometric analysis and lesion profile were performed using the Prism software. Normal distribution of data was assessed by D'Agostino-Pearson normality test. The differences in normalized serpins transcript ΔC_T values between SerpinA3n$^{-/-}$ and SerpinA3n$^{+/+}$ animals, as well as between prion-infected SerpinA3n$^{-/-}$ and SerpinA3n$^{+/+}$ animals, were evaluated using the Mann-Whitney test. A *p*-value of <0.05 was considered statistically significant.

CRediT authorship contribution statement

Fabio Moda: Writing – original draft, Supervision, Resources, Methodology, Funding acquisition, Data curation, Conceptualization. **Chiara Ferracin:** Writing – review & editing, Visualization, Methodology, Investigation, Formal analysis, Data curation. **Ilaria Linda Dellarole:** Writing – review & editing, Visualization, Methodology, Formal

analysis, Conceptualization. **Edoardo Bistaffa:** Writing – review & editing, Visualization, Methodology, Formal analysis, Data curation. **Chiara Maria Giulia De Luca:** Writing – review & editing, Visualization, Methodology, Formal analysis, Data curation. **Marco Zattoni:** Writing – review & editing, Visualization, Methodology, Formal analysis, Data curation. **Diletta Giovanna Legari:** Writing – review & editing, Visualization, Methodology, Formal analysis, Data curation. **Lea Nikolic:** Writing – review & editing, Visualization, Methodology, Formal analysis, Data curation. **Anna Burato:** Writing – review & editing, Visualization, Methodology, Formal analysis, Data curation. **Martina Brce:** Writing – review & editing, Visualization, Methodology, Formal analysis, Data curation. **Giuseppe Bufano:** Writing – review & editing, Visualization, Methodology, Formal analysis, Data curation. **Merve Begüm Bacınoğlu:** Writing – review & editing, Visualization, Methodology, Formal analysis, Data curation. **Federico Angelo Cazzaniga:** Writing – review & editing, Visualization, Methodology, Formal analysis, Data curation. **Tihana Lenac Rovis:** Methodology, Data curation. **Giuseppe Legname:** Writing – original draft, Supervision, Methodology, Data curation, Conceptualization.

Funding information

This work was partially supported by the Italian Ministry of Health (grant number RRC) and Associazione Italiana Encefalopatie da Prioni (AIEnP) to FM.

Declaration of competing interest

The authors declare that they have no conflicts of interest with the contents of this article.

Appendix A. Supplementary data

Supplementary data to this article can be found online at https://doi.org/10.1016/j.nbd.2025.106973.

Data availability

Data will be made available on request.

References

Aguzzi, A., 2006 Jun. Prion diseases of humans and farm animals: epidemiology, genetics, and pathogenesis. J. Neurochem. 97 (6), 1726–1739.
Angelucci, F., Veverova, K., Katonová, A., Piendel, L., Vyhnalek, M., Hort, J., 2022 Aug. Alzheimer's disease severity is associated with an imbalance in serum levels of enzymes regulating plasmin synthesis. Pharmaceuticals 15 (9), 1074.
Baker, C., 2007. SERPINA3 (aka alpha-1-antichymotrypsin). Front. Biosci. 12 (8–12), 2821.
Barbisin, M., Vanni, S., Schmädicke, A.-C., Montag, J., Motzkus, D., Opitz, L., et al., 2014 Dec. Gene expression profiling of brains from bovine spongiform encephalopathy (BSE)-infected cynomolgus macaques. BMC Genomics 15 (1), 434.
Benetti, F., Gustincich, S., Legname, G., 2012 Mar. Gene expression profiling and therapeutic interventions in neurodegenerative diseases: a comprehensive study on potentiality and limits. Expert Opin. Drug Discov. 7 (3), 245–259.
Bistaffa, E., Rossi, M., De Luca, C.M.G., Cazzaniga, F., Carletta, O., Campagnani, I., et al., 2019 Nov. Prion efficiently replicates in α-synuclein knockout mice. Mol. Neurobiol. 56 (11), 7448–7457.
Bodemer, W., 2016 Sep. Prions. Primate Biol. 3 (2), 47–50.
Bruce, M.E., McConnell, I., Fraser, H., Dickinson, A.G., 1991 Mar. The disease characteristics of different strains of scrapie in Sinc congenic mouse lines: implications for the nature of the agent and host control of pathogenesis. J. Gen. Virol. 72 (3), 595–603.
Campbell, I.L., Eddleston, M., Kemper, P., Oldstone, M.B., Hobbs, M.V., 1994 Apr. Activation of cerebral cytokine gene expression and its correlation with onset of reactive astrocyte and acute-phase response gene expression in scrapie. J. Virol. 68 (4), 2383–2387.
Chesebro, B., 1999 Nov. Prion protein and the transmissible spongiform encephalopathy diseases. Neuron 24 (3), 503–506.
Colini Baldeschi, A., Zattoni, M., Vanni, S., Nikolic, L., Ferracin, C., La Sala, G., et al., 2022 Jul. Innovative non-PrP-targeted drug strategy designed to enhance prion clearance. J. Med. Chem. 65 (13), 8998–9010.
Constantinescu, P., Brown, R.A., Wyatt, A.R., Ranson, M., Wilson, M.R., 2017 Sep. Amorphous protein aggregates stimulate plasminogen activation, leading to release of cytotoxic fragments that are clients for extracellular chaperones. J. Biol. Chem. 292 (35), 14425–14437.
Cortes-Canteli, M., Paul, J., Norris, E.H., Bronstein, R., Ahn, H.J., Zamolodchikov, D., et al., 2010 Jun. Fibrinogen and β-amyloid association alters thrombosis and fibrinolysis: a possible contributing factor to Alzheimer's disease. Neuron 66 (5), 695–709.
D'Acunto, E., Fra, A., Visentin, C., Manno, M., Ricagno, S., Galliciotti, G., et al., 2021 Oct. Neuroserpin: structure, function, physiology and pathology. Cell. Mol. Life Sci. 78 (19–20), 6409–6430.
Dandoy-Dron, F., Benboudjema, L., Guillo, F., Jaegly, Alexandre, Jasmin, C., Dormont, D., et al., 2000 Mar. Enhanced levels of scrapie responsive gene mRNA in BSE-infected mouse brain. Mol. Brain Res. 76 (1), 173–179.
Das, S., Potter, H., 1995 Feb. Expression of the Alzheimer amyloid-promoting factor antichymotrypsin is induced in human astrocytes by IL-1. Neuron 14 (2), 447–456.
Elliott, P.R., Pei, X.Y., Dafforn, T.R., Lomas, D.A., 2000 Jan. Topography of a 2.0 Å structure of α 1 -antitrypsin reveals targets for rational drug design to prevent conformational disease. Protein Sci. 9 (7), 1274–1281.
Eriksson, S., Lindmark, B., Lilja, H., 1986 Jan. Familial α 1 -antichymotrypsin deficiency. Acta Med. Scand. 220 (5), 447–453.
Forsyth, S., Horvath, A., Coughlin, P., 2003 Mar. A review and comparison of the murine α1-antitrypsin and α1-antichymotrypsin multigene clusters with the human clade A serpins. Genomics 81 (3), 336–345.
Fraser, H., 1993 Oct. Diversity in the neuropathology of scrapie-like diseases in animals. Br. Med. Bull. 49 (4), 792–809.
Fraser, H., Dickinson, A.G., 1967 Dec. Distribution of experimentally induced scrapie lesions in the brain. Nature 216 (5122), 1310–1311.
Fraser, H., Dickinson, A.G., 1968 Jul. The sequential development of the brain lesions of scrapie in three strains of mice. J. Comp. Pathol. 78 (3), 301–311. Available from: https://linkinghub.elsevier.com/retrieve/pii/0021997568900066.
Fraser, H., Dickinson, A.G., 1973 Jan. Scrapie in mice. J. Comp. Pathol. 83 (1), 29–40.
Haass, C., 2004 Feb. Take five—BACE and the γ-secretase quartet conduct Alzheimer's amyloid β-peptide generation. EMBO J. 23 (3), 483–488.
Heit, C., Jackson, B.C., McAndrews, M., Wright, M.W., Thompson, D.C., Silverman, G.A., et al., 2013 Dec. Update of the human and mouse SERPINgene superfamily. Hum. Genomics 7 (1), 22.
Higashiyama, M., Doi, O., Yokouchi, H., Kodama, K., Nakamori, S., Tateishi, R., 1995 Oct. Alpha-1-antichymotrypsin expression in lung adenocarcinoma and its possible association with tumor progression. Cancer 76 (8), 1368–1376.
Horvath, A.J., Forsyth, S.L., Coughlin, P.B., 2004 Oct. Expression patterns of murine antichymotrypsin-like genes reflect evolutionary divergence at the Serpina3 locus. J. Mol. Evol. 59 (4), 488–497.
Hwang, S.-R., Steineckert, B., Kohn, A., Palkovits, M., Hook, V.Y.H., 1999 Jan. Molecular studies define the primary structure of α1-antichymotrypsin (ACT) protease inhibitor in Alzheimer's disease brains. J. Biol. Chem. 274 (3), 1821–1827.
Kascsak, R.J., Rubenstein, R., Merz, P.A., Carp, R.I., Wisniewski, H.M., Diringer, H., 1985 Aug. Biochemical differences among scrapie-associated fibrils support the biological diversity of scrapie agents. J. Gen. Virol. 66 (8), 1715–1722.
Kascsak, R.J., Rubenstein, R., Merz, P.A., Carp, R.I., Robakis, N.K., Wisniewski, H.M., et al., 1986 Sep. Immunological comparison of scrapie-associated fibrils isolated from animals infected with four different scrapie strains. J. Virol. 59 (3), 676–683.
Koomen, J.M., Shih, L.N., Coombes, K.R., Li, D., Xiao, L., Fidler, I.J., et al., 2005 Feb. Plasma protein profiling for diagnosis of pancreatic cancer reveals the presence of host response proteins. Clin. Cancer Res. 11 (3), 1110–1118.
Kordula, T., Rydel, R.E., Brigham, E.F., Horn, F., Heinrich, P.C., Travis, J., 1998 Feb. Oncostatin M and the interleukin-6 and soluble interleukin-6 receptor complex regulate α1-antichymotrypsin expression in human cortical astrocytes. J. Biol. Chem. 273 (7), 4112–4118.
Kordula, T., Bugno, M., Rydel, R.E., Travis, J., 2000 Oct. Mechanism of interleukin-1- and tumor necrosis factor α-dependent regulation of the α 1 -antichymotrypsin gene in human astrocytes. J. Neurosci. 20 (20), 7510–7516.
Ledesma, M.D., Da Silva, J.S., Crassaerts, K., Delacourte, A., De Strooper, B., Dotti, C.G., 2000 Dec. Brain plasmin enhances APP α-cleavage and Aβ degradation and is reduced in Alzheimer's disease brains. EMBO Rep. 1 (6), 530–535.
Legname, G., Virgilio, T., Bistaffa, E., De Luca, C.M.G., Catania, M., Zago, P., et al., 2018 Mar. Effects of peptidyl-prolyl isomerase 1 depletion in animal models of prion diseases. Prion 12 (2), 127–137.
Leinonen, J., Lövgren, T., Vornanen, T., Stenman, U.H., 1993 Oct. Double-label time-resolved immunofluorometric assay of prostate-specific antigen and of its complex with alpha 1-antichymotrypsin. Clin. Chem. 39 (10), 2098–2103.
Livak, K.J., Schmittgen, T.D., 2001 Dec. Analysis of relative gene expression data using real-time quantitative PCR and the 2−ΔΔCT method. Methods 25 (4), 402–408.
Mahadeva, R., 2001 Jan. Association of alpha1-antichymotrypsin deficiency with milder lung disease in patients with cystic fibrosis. Thora 56 (1), 53–58.
Miele, G., Seeger, H., Marino, D., Eberhard, R., Heikenwalder, M., Stoeck, K., et al., 2008 Dec. In: Graeber, M.B. (Ed.), Urinary α1-Antichymotrypsin: A Biomarker of Prion Infection, PLoS One, 3(12):e3870.
Morales, R., Abid, K., Soto, C., 2007. The prion strain phenomenon: molecular basis and unprecedented features. Biochim. Biophys. Acta Mol. basis Dis.
Naidoo, N., Cooperman, B.S., Wang, Z., Liu, X., Rubin, H., 1995 Jun. Identification of Lysines within α1-antichymotrypsin important for DNA binding. An unusual combination of DNA-binding elements. J. Biol. Chem. 270 (24), 14548–14555.
Prusiner, S.B., Scott, M.R., DeArmond, S.J., Cohen, F.E., 1998 May. Prion protein biology. Cell 93 (3), 337–348.

Rubenstein, R., Merz, P.A., Kascsak, R.J., Scalici, C.L., Papini, M.C., Carp, R.I., et al., 1991 Jul. Scrapie-infected spleens: analysis of infectivity, scrapie-associated fibrils, and protease-resistant proteins. J. Infect. Dis. 164 (1), 29–35.
Sejvar, J.J., Schonberger, L.B., Belay, E.D., 2008 Dec. Transmissible spongiform encephalopathies. J. Am. Vet. Med. Assoc. 233 (11), 1705–1712.
Solforosi, L., Milani, M., Mancini, N., Clementi, M., Burioni, R., 2013 Mar. A closer look at prion strains. Prion 7 (2), 99–108.
Sun, Y., Wright, H.T., Janciauskiene, S., 2002 Feb. α1-Antichymotrypsin/Alzheimer's peptide Aβ 1–42 complex perturbs lipid metabolism and activates transcription factors PPARγ and NFκB in human neuroblastoma (Kelly) cells. J. Neurosci. Res. 67 (4), 511–522.
Truett, G.E., Heeger, P., Mynatt, R.L., Truett, A.A., Walker, J.A., Warman, M.L., 2000 Jul. Preparation of PCR-quality mouse genomic DNA with hot sodium hydroxide and Tris (HotSHOT). Biotechniques 29 (1), 52–54.
Turk, E., Teplow, D.B., Hood, L.E., Prusiner, S.B., 1988 Sep. Purification and properties of the cellular and scrapie hamster prion proteins. Eur. J. Biochem. 176 (1), 21–30.
Vanni, S., Moda, F., Zattoni, M., Bistaffa, E., De Cecco, E., Rossi, M., et al., 2017. Differential overexpression of SERPINA3 in human prion diseases. Sci. Rep. 7 (1), 15637.
Vanni, S., Zattoni, M., Moda, F., Giaccone, G., Tagliavini, F., Haïk, S., et al., 2018. Jan. Hemoglobin mRNA changes in the frontal cortex of patients with neurodegenerative diseases. Front. Neurosci. 12, 8.
Wulf, M.-A., Senatore, A., Aguzzi, A., 2017 Dec. The biological function of the cellular prion protein: an update. BMC Biol. 15 (1), 34.
Xiang, W., Windl, O., Wünsch, G., Dugas, M., Kohlmann, A., Dierkes, N., et al., 2004 Oct. Identification of differentially expressed genes in scrapie-infected mouse brains by using global gene expression technology. J. Virol. 78 (20), 11051–11060.
Yamamura, J., Miyoshi, Y., Tamaki, Y., Taguchi, T., Iwao, K., Monden, M., et al., 2004. mRNA expression level of estrogen-inducible gene, α 1-antichymotrypsin, is a predictor of early tumor recurrence in patients with invasive breast cancers. Cancer Sci. 95 (11), 887–892.
Zattoni, M., Mearelli, M., Vanni, S., Colini Baldeschi, A., Tran, T.H., Ferracin, C., et al., 2022 Jun. Serpin signatures in prion and Alzheimer's diseases. Mol. Neurobiol. 59 (6), 3778–3799.